The genomic DNA samples from the six patients were treated with the MethylEasy Xceed Rapid DNA Bisulphite Modification Kit (Human Genetics Signatures Pty Ltd, Australia), according to the manufacturer's instructions. The methylation and unmethylation primers for POTAGE were designed using the CpG island searcher (http://cpgislands.usc.edu/) (Takai and Jones, 2003) and MethPrimer (http://www.urogene.org/methprimer/index1.html) web sites (Li and Dahiya, 2002). After the amplification, the PCR products were separated by electrophoresis on an agarose gel, and fragments in the expected range were excised and purified using the QIAquick Gel Extraction Kit (Qiagen, Valencia, CA). The purified PCR products were ligated using the pGEM-T Easy Vector System (Promega, WI, USA), and at least 20 independent clones were sequenced with the T7 (5′-TAATACGACTCACTATAGGG-3′) and SP6 (5′-ATTTAGGTGACACTATAGAA-3′) primers.

3. Results

3.1. Analysis of tiling array data

Our goal was to evaluate all the mRNAs expressed in human prostate cells, using the tiling array in triplicate. The signal intensity and P-value for each probe were determined by quantile normalization (Bolstad et al., 2003), after the raw intensity data from triplicate microarrays were transformed with the Affymetrix Tiling Analysis Software ver. 1.1. All of the extracted signal data were mapped to their genomic position and visualized in the IGB. Because the tiling array was designed based on information from NCBI Build 34, the results were translated to Build 36 automatically.

Because the thresholds determining positive signal intensity were determined on the basis of the signals from all the probes in each tiling array, the thresholds were slightly different for each array (see Materials and methods). The values for two other parameters (Max gap and Min run) were the same for all the arrays (see Materials and methods). The three parameter settings enabled us to predict the genomic locations likely to contain transcribed sequences. After comparing the sequences from our predicted regions with those of annotated genes (NCBI Build 37.1), we found 319 regions in the entire genomic sequence that encoded undiscovered transcripts. After the novel regions were obtained, the novel zones were defined by tiling data analysis. Finally, we defined 17 zones containing two or more regions within 5-kbp of each other (Fig. 1A, Supplemental Fig. 1 and Supplemental Table 1).

3.2. RT-PCR and RACE analysis of the novel region of human chromosome 12

We next designed primer sets for each region that were appropriate for performing RT-PCR analysis with the single-strand cDNA obtained from normal prostate cells. Each RT-PCR product was sequenced to confirm the amplification of the target sequences. Even when a positive tiling array signal was confirmed, no region was studied further without the successful amplification of the correct sequence. In addition, single regions that did not have any positive regions in the flanking regions were also excluded. After the RT-PCR analysis, primers for 5′- and 3′-RACE were designed on the basis of both the tiling array data and information from NCBI Build 37.1. All of the 5′- and 3′-RACE experiments were performed with single-stranded cDNA obtained from normal human prostate tissue.

Finally, we obtained the full-length sequence of POTAGE on chromosome 12q24.13 (Supplemental Table 2, primer Nos. 1–4, Supplemental Figs. 4, 5). However we succeeded to obtain the 17 zones by tiling array data, we failed to confirm 16 zones by RT-PCR and/or RACE.

The novel mRNA sequence we obtained consisted of 26 exons within an mRNA of 5841 bp. The gene was located on chromosome 12q24.13. Assuming that the tiling array data might indicate one of the exons in the novel transcripts, we performed RT-PCR and RACE of the regions in this zone. From these results, we found that 4 of the 6 5′-most exons of POTAGE belonged to the hypothetical protein LOC100287871 (http://www.ncbi.nlm.nih.gov/gene/?term=LOC100287871). Moreover, 18 of the 19 3′-most exons overlapped with part of the 5′-end of predicted gene C12orf51 in NCBI Build 37.1. There were three novel exons in POTAGE: exons 1, 10, and 26. Exon 23 of POTAGE contained a 30-bp deletion compared with the 5′-end of C12orf51 exon 22. The remaining 22 exons of POTAGE shared 100% identity with C12orf51 (Figs. 1B–F, Supplemental Table 3).

We also investigated the sequence flanking exons 25 and 26 of POTAGE in detail. We found at least two human isoforms of these exons. One isoform included exon 26 of POTAGE as its 3′-end; this isoform was equivalent to POTAGE. The other isoform had a different 3′-end; that is, some other exon followed exon 25. For example, C12orf51 was partially encoded by the other isoform.

To explore the possible function of POTAGE, motif and homology searches were performed using the MOTIF Search (http://motif.genome.jp/), Pfam (http://pfam.sanger.ac.uk/), and NCBI web sites. No major motif was found in the nucleotide acid sequence or the deduced protein sequence.

3.3. Comparison of POTAGE expression level in multiple human tissues

We evaluated the expression levels of POTAGE with region-specific primer pairs in multiple human tissues (Human MTC Panels I and II), using semi-quantitative real-time RT-PCR (Supplemental Table 2, primer No. 5). POTAGE was expressed in every human tissue examined. The relative expression levels were calculated as the levels normalized to the beta-actin expression in each sample. The highest expression level of POTAGE was observed in the testis (Fig. 2). We created primer pairs to evaluate the level of expression of the other isoform, and performed real time RT-PCR using the same conditions as for POTAGE. While the expression level of the other isoform also was higher in testis, it was different from that of POTAGE, in that the other isoform was also highly expressed in skeletal muscle (data not shown).

3.4. Methylation assay for the 5′-upstream CG-rich region of POTAGE

Because DNA methylation in the 5′-upstream CG-rich region of a gene is related to the repression of gene expression, we investigated the methylation status of POTAGE using a methylation-specific PCR assay, to discover if differences in methylation could explain the lower expression level of POTAGE in normal prostate tissue compared to other tissues (Jones and Baylin, 2007; Laird, 2003; Ting et al., 2006;

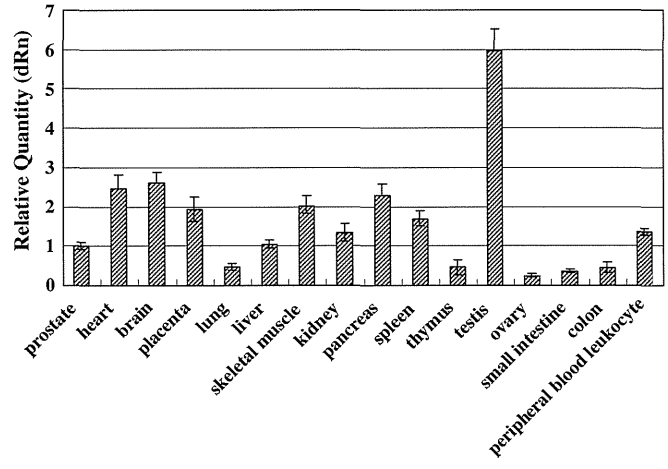

Fig. 2. The expression levels of the novel gene in multiple human tissues using semi-quantitative real-time RT-PCR. The novel gene was expressed in every human tissue examined in this study, and its level was highest in the testis.

Table 1
Homology among exons of the novel gene in human, mouse, rat, and fugu (pufferfish).

		cDNA (translated region)			
		Human	Mouse	Rat	Fugu
Amino acids	Human		89.18%	88.80%	70.60%
	Mouse	97.27%		95.14%	72.59%
	Rat	97.05%	98.19%		72.47%
	Fugu	81.15%	81.00%	80.92%	

The percentage of identical amino acids was essentially constant across species.

Vanaja et al., 2009). In addition, we examined the methylation condition in prostate cancer tissue, to assess any relationship between the level of expression and prostate oncogenesis. We examined the methylation of CpG 101 (UCSC (http://genome.ucsc.edu/) GRCh37/hg39), a CpG island located 557 bp upstream of POTAGE (Supplemental Table 2, Nos. 6–7, Supplemental Fig. 6). However, the CpG island was not methylated in normal or cancerous prostate tissues.

4. Discussion

New genomic technologies have yielded much useful information about the whole human genome, and both experimental and computational approaches have been developed to handle the accumulation of data. Our approach using the tiling array supported the importance of choosing the appropriate settings for the three parameters, threshold of signal intensity, Max gap, and Min run, when examining the tiling data to evaluate mRNA expression or discover novel genes. The settings of these parameters were critical to our finding the few pieces of relevant information among the enormous quantities of tiling array data. Because our data demonstrated that the signal patterns of many undiscovered regions were very short or very close to annotated genes, we excluded unknown regions with these patterns to obtain novel genes that were independent of the known genes. Therefore, the three parameters in our data were chosen to be stringent, to reduce the amount of data that would require further investigation.

First, our parameter settings allowed us to extract 17 zones containing novel regions from our entire set of tiling array data. All of the zones consisted of two or more novel regions within about 5-kbp of one another. We assumed that each novel region might represent one or more exons of a novel gene. In 16 of the 17 zones, each region was confirmed as encoding a transcript. However, no amplification product included neighboring sequences.

Finally, we determined the sequence of a full-length novel gene from the RT-PCR and RACE results of 1 of the 17 zones. The novel mRNA was 5841 bp in length and contained 26 exons, which were encoded by sequences spread over 133,876 bp in the genome, on chromosome 12q24.13. There were two predicted genes, hypothetical protein LOC100287871 and C12orf51, that were close to our discovered gene (NCBI Build 36.3). The information on hypothetical protein LOC100287871 was replaced with the predicted region of C12orf51 in NCBI Build 37.1. To confirm the sequence of POTAGE, we also referred to the sequence of the predicted transcript at NCBI Build 37.1.

Among the 26 exons of POTAGE, three were novel (exons 1, 10, and 26). POTAGE also shared 23 exons with C12orf51 (NCBI Build 37.1), and the 22nd exon of POTAGE (the 23rd exon of C12orf51) contained a 30-bp deletion.

The expression level of POTAGE was lower in the prostate than in most other tissues. To investigate whether POTAGE's expression was suppressed by methylation, we examined the genomic methylation in the 5′-upstream CpG island of POTAGE in normal prostate and prostate cancer, to look for possible associations between malignancies and expression of POTAGE. However, the region we assayed was not methylated in normal or cancerous prostate tissue. Therefore, the different expression levels in several tissues, including prostate cancer, are unlikely to be regulated by the methylation of the 5′-upstream CG rich region of POTAGE.

POTAGE has no major motif in the nucleotide acid sequence or the deduced protein sequence. Interestingly, the sequence of POTAGE had high homology to transcripts in other species, such as mouse and rat. The predicted protein had a 97% sequence identity between human and mouse, and almost the same homology between human and rat (Table 1). The alignment of the amino acid sequences, which was constructed using CLUSTAL W ver. 1.83 (http://clustalw.ddbj.nig.ac.jp/top-j.html) with Kimura's correction, between human and five other species, showed the closest matches among different species (Supplemental Fig. 7). Furthermore, the phylogenetic relationship based on the amino acid alignments of these six species also revealed high protein homology among human and other species (Fig. 3). On the other hand, the nucleotide sequence identities between human and mouse of two housekeeping proteins (beta-Actin and GAPDH) are 92% and 89%. The between-species percent identity of POTAGE was higher than that of these housekeeping genes. Therefore, although the function of POTAGE is currently unknown, its high sequence homology among different species suggests that it may have an important or essential biological function.

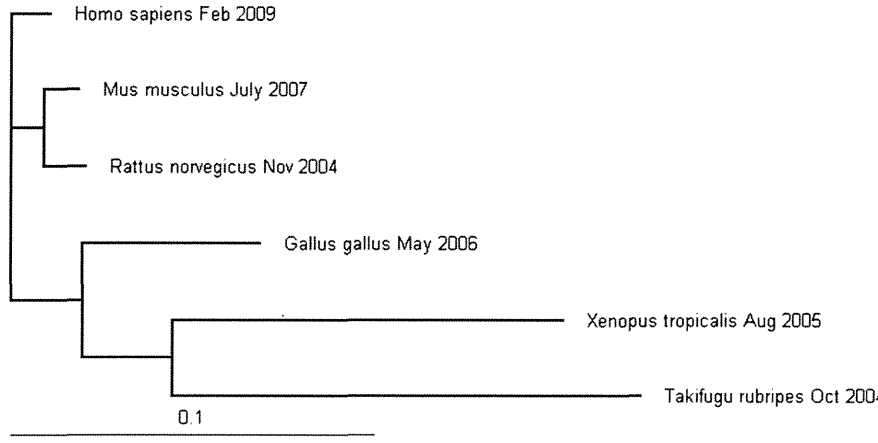

Fig. 3. Phylogram depicting the relationship between the deduced amino acid sequence encoded by the novel gene in humans and its homologues in five other species, using Tree View (ver. 1.6.6). The phylogram was based on the alignment of the amino acid sequences (see Supplemental Fig. 7).

In summary, we identified a novel gene in a search of the whole human genome using the powerful new tiling array tool. Although analyzing the tiling array data was no simple matter, it was still useful for detecting a novel gene.

Supplementary data to this article can be found online at http://dx.doi.org/10.1016/j.gene.2012.11.076.

Acknowledgments

T. Ichikawa is thanked for excellent secretarial assistance. R. Sato and F. Sato (SASA Plus Co., Ltd., Fukuoka, Japan) are thanked for the assistant of data management and the development of the specific tool for sequence analysis. This work was supported by grants from Grants-in-Aid for Scientific Research.

References

Bertone, P., et al., 2004. Global identification of human transcribed sequences with genome tiling arrays. Science 306, 2242–2246.
Bolstad, B.M., Irizarry, R.A., Astrand, M., Speed, T.P., 2003. A comparison of normalization methods for high density oligonucleotide array data based on variance and bias. Bioinformatics 19, 185–193.
Castellano, L., et al., 2009. The estrogen receptor-alpha-induced microRNA signature regulates itself and its transcriptional response. Proc. Natl. Acad. Sci. U. S. A. 106, 15732–15737.
Cheng, J., et al., 2005. Transcriptional maps of 10 human chromosomes at 5-nucleotide resolution. Science 308, 1149–1154.
Eisenberg, E., Levanon, E.Y., 2003. Human housekeeping genes are compact. Trends Genet. 19, 362–365.
Heintzman, N.D., et al., 2009. Histone modifications at human enhancers reflect global cell-type-specific gene expression. Nature 459, 108–112.
Hussain, M., et al., 2009. Tobacco smoke induces polycomb-mediated repression of Dickkopf-1 in lung cancer cells. Cancer Res. 69, 3570–3578.
International Human Genome Sequencing Consortium, 2004. Finishing the euchromatic sequence of the human genome. Nature 431, 931–945.
Johnson, J.M., Edwards, S., Shoemaker, D., Schadt, E.E., 2005. Dark matter in the genome: evidence of widespread transcription detected by microarray tiling experiments. Trends Genet. 21, 93–102.
Jones, P.A., Baylin, S.B., 2007. The epigenomics of cancer. Cell 128, 683–692.
Kampa, D., et al., 2004. Novel RNAs identified from an in-depth analysis of the transcriptome of human chromosomes 21 and 22. Genome Res. 14, 331–342.
Kapranov, P., et al., 2002. Large-scale transcriptional activity in chromosomes 21 and 22. Science 296, 916–919.
Kapranov, P., et al., 2005. Examples of the complex architecture of the human transcriptome revealed by RACE and high-density tiling arrays. Genome Res. 15, 987–997.
Laird, P.W., 2003. The power and the promise of DNA methylation markers. Nat. Rev. Cancer 3, 253–266.
Lander, E.S., et al., 2001. Initial sequencing and analysis of the human genome. Nature 409, 860–921.
Li, L.C., Dahiya, R., 2002. MethPrimer: designing primers for methylation PCRs. Bioinformatics 18, 1427–1431.
Mockler, T.C., Chan, S., Sundaresan, A., Chen, H., Jacobsen, S.E., Ecker, J.R., 2005. Applications of DNA tiling arrays for whole-genome analysis. Genomics 85, 1–15.
Nelson, C.M., et al., 2008. Whole genome transcription profiling of *Anaplasma phagocytophilum* in human and tick host cells by tiling array analysis. BMC Genomics 9, 364.
Nicol, J.W., Helt, G.A., Blanchard Jr., S.G., Raja, A., Loraine, A.E., 2009. The Integrated Genome Browser: free software for distribution and exploration of genome-scale datasets. Bioinformatics 25, 2730–2731.
Royce, T.E., et al., 2005. Issues in the analysis of oligonucleotide tiling microarrays for transcript mapping. Trends Genet. 21, 466–475.
Sasaki, D., Kondo, S., Maeda, N., Gingeras, T.R., Hasegawa, Y., Hayashizaki, Y., 2007. Characteristics of oligonucleotide tiling arrays measured by hybridizing full-length cDNA clones: causes of signal variation and false positive signals. Genomics 89, 541–551.
Schadt, E.E., et al., 2004. A comprehensive transcript index of the human genome generated using microarrays and computational approaches. Genome Biol. 5, R73.
Shoemaker, D.D., et al., 2001. Experimental annotation of the human genome using microarray technology. Nature 409, 922–927.
Takai, D., Jones, P.A., 2003. The CpG island searcher: a new WWW resource. Silico Biol, 3, pp. 235–240.
Takata, R., Akamatsu, S., Kubo, M., Takahashi, A., Hosono, N., Kawaguchi, T., Tsunoda, T., Inazawa, J., Kamatani, N., Ogawa, O., Fujioka, T., Nakamura, Y., Nakagawa, H., 2010. Genome-wide association study identifies five new susceptibility loci for prostate cancer in the Japanese population. Nat. Genet. 42, 751–754.
Ting, A.H., McGarvey, K.M., Baylin, S.B., 2006. The cancer epigenome—components and functional correlates. Genes Dev. 20, 3215–3231.
Vanaja, D.K., et al., 2009. Hypermethylation of genes for diagnosis and risk stratification of prostate cancer. Cancer Invest. 27, 549–560.
Venter, J.C., et al., 2001. The sequence of the human genome. Science 291, 1304–1351.
Weile, C., Gardner, P.P., Hedegaard, M.M., Vinther, J., 2007. Use of tiling array data and RNA secondary structure predictions to identify noncoding RNA genes. BMC Genomics 8, 244.
Xu, J., et al., 2005. A combined genomewide linkage scan of 1,233 families for prostate cancer-susceptibility genes conducted by the international consortium for prostate cancer genetics. Am. J. Hum. Genet. 77, 219–229.
Yeager, M., et al., 2007. Genome-wide association study of prostate cancer identifies a second risk locus at 8q24. Nat. Genet. 39, 645–649.
Yeager, M., et al., 2009. Identification of a new prostate cancer susceptibility locus on chromosome 8q24. Nat. Genet. 41, 1055–1057.

Proteomic Pattern Analysis Discriminates Among Multiple Sclerosis–Related Disorders

Mika Komori, MD,[1] Yumiko Matsuyama, PhD,[2] Takashi Nirasawa, PhD,[2] Herbert Thiele, PhD,[3] Michael Becker, PhD,[3] Theodore Alexandrov, PhD,[4] Takahiko Saida, MD, PhD,[5] Masami Tanaka, MD, PhD,[5] Hidenori Matsuo, MD, PhD,[6] Hidekazu Tomimoto, MD, PhD,[1] Ryosuke Takahashi, MD, PhD,[1] Kei Tashiro, MD, PhD,[7] Masaya Ikegawa, MD, PhD,[7] and Takayuki Kondo, MD, PhD[8]

Objective: To use a new, unbiased biomarker discovery strategy to obtain and assess proteomic data from cerebrospinal fluid (CSF) of patients with multiple sclerosis (MS)-related disorders.
Methods: CSF protein profiles were analyzed from 107 patients with either MS-related disorders (including relapsing remitting MS [RRMS], primary progressive MS [PPMS], anti-aquaporin4 antibody seropositive–neuromyelitis optica spectrum disorder [SP-NMOSD], and seronegative-NMOSD with long cord lesions on spinal magnetic resonance imaging [SN-NMOSD]), amyotrophic lateral sclerosis (ALS), or other inflammatory neurological diseases (used as controls). CSF peptides/proteins were purified with magnetic beads, and directly measured by matrix-assisted laser desorption/ionization time-of-flight mass spectrometry. The obtained spectra were analyzed with multivariate statistics and pattern matching algorithms. These analyses were replicated in an independent sample set of 84 patients composed of those with MS-related disorders or with other neurological diseases (the second cohort).
Results: MS-related disorders differed considerably in terms of CSF protein profiles. SP-NMOSD and SN-NMOSD, both of which fit within the NMO spectrum, were distinguishable from RRMS with high cross-validation accuracy on a support vector machine classifier, especially in relapse phases. Some peaks derived from samples of relapsed SP-NMOSD can discriminate RRMS with high area under curve scores (>0.95) and this was reproduced on the second cohort. The similarity of proteomic patterns between selected neurological diseases were demonstrated by pattern matching analysis. To our surprise, the spectral differences between RRMS and PPMS were much larger than those of PPMS and ALS.
Interpretation: Our findings suggest that CSF proteomic pattern analysis can increase the accuracy of disease diagnosis of MS-related disorders and will aid physicians in appropriate therapeutic decision-making.

ANN NEUROL 2012;71:614–623

Multiple sclerosis (MS)-related disorders are inflammatory diseases of the central nervous system (CNS), and are characterized by different degrees of autoimmune involvement and neurodegeneration.[1] Categories of MS-related disorders include relapsing-remitting MS (RRMS), secondary progressive MS (SPMS), primary progressive MS (PPMS), progressive relapsing MS (PRMS), Balo's concentric sclerosis, and neuromyelitis optica (NMO). It is crucial to differentially diagnose these disorders in order to select the appropriate treatment course that will benefit the patient. Since effective therapy has only been established for RRMS, it is

View this article online at wileyonlinelibrary.com. DOI: 10.1002/ana.22633

Received Oct 16, 2010, and in revised form Aug 29, 2011. Accepted for publication Sep 2, 2011.

Address correspondence to Dr Masaya Ikegawa, Department of Genomic Medical Sciences, Graduate School of Medical Science, Kyoto Prefectural University of Medicine, Kajii-cho 465 Kawaramachi Hirokoji, Kamigyo-ku, Kyoto, Japan, 602-8566. E-mail: mikegawa@koto.kup-m.ac.jp

From the [1]Department of Neurology, Graduate School of Medicine, Kyoto University, Kyoto, Japan; [2]Bruker Daltonics K.K., Yokohama, Japan; [3]Bruker Daltonik GmbH, Bremen, Germany; [4]Center for Industrial Mathematics, University of Bremen, Bremen, Germany; [5]Department of Neurology, Utano National Hospital, Kyoto, Japan; [6]Division of Clinical Research, Nagasaki Medical Center of Neurology, Nagasaki, Japan; [7]Department of Genomic Medical Sciences, Graduate School of Medicine, Kyoto Prefectural University of Medicine, Kyoto, Japan; and [8]The Tazuke Kofukai Medical Research Institute, Kitano Hospital, Osaka, Japan.

Additional Supporting Information can be found in the online version of this article.

necessary that we gain a comprehensive understanding of how RRMS pathogenesis is similar to the other MS-related disorders so that similarly efficacious treatments may be developed. It is particularly important to differentiate RRMS and NMO, given their largely overlapping clinical characteristics, their particular prevalence in East Asia, and because the optimal treatments for the diseases differ considerably.[2,3] The current Mayo NMO diagnostic criteria[4] requires clinical episodes of both optic neuritis and myelitis to definitively identify NMO. Anti-aquaporin-4 (AQP4) antibody was discovered as a biomarker of NMO[5,6]; however, this designation has evoked some controversy. First, the clinical spectrum of disorders defined by the presence of anti-AQP4 antibody[2] encompasses recurrent optic neuritis or myelitis alone and Asian "optic-spinal MS" with long cord lesion (LCL) on spinal magnetic resonance imaging (MRI),[2,7] which are not included in the 2006 Mayo NMO criteria.[4] NMO-specific brain lesions have also been classified.[8] Second, although LCL is 1 of the most characteristic features of NMO, a considerable number of subjects with LCL present as seronegative for the anti-AQP4 antibody. Even for those patients fulfilling the 2006 Mayo NMO criteria, 24% to 67% have been reported as being seronegative for the anti-AQP4 antibody.[4,5,9,10] Although the term "NMO spectrum disorder (NMOSD)" has been used for these disorders, it is not clear whether these seronegative subjects are the result of inadequate clinical diagnostic criteria, suboptimal assay sensitivity, or different targeted antigens. Moreover, it remains unknown whether seropositive and seronegative NMO patients have shared or distinct pathogenesis.

PPMS carries a poor prognosis, and no successful therapeutic trials have been accomplished to date.[11] The notion that RRMS and PPMS can be treated as a single disorder is unproven, although sufficiently large and lengthy research studies are underway.[12] It is necessary to know whether the 2 forms of MS have distinct pathogeneses as they may require different therapeutic strategies. It also remains uncertain, although it has been speculated, that the progressive form of MS undergoes more significant neurodegeneration than does the relapsing form of MS.[13]

The cerebrospinal fluid (CSF) is considered by many to be a window into the brain through which one might identify promising new biomarkers of neurodegenerative disorders. Indeed, several biomarkers for MS-related disorders have been reported from studies on CSF.[14–22] Recently, CSF glial fibrillary acidic protein (CSF-GFAP) and S100B were proposed as promising biomarker candidates of NMO attacks.[23] CSF-GFAP was found to be elevated more than 1,000-fold in NMO patients, as compared to control cases, and the increased concentrations were determined to be the result of astrocyte destruction. However, complex traits of MS-related disorders defy strict association with a single biological process. CSF-GFAP elevation can result from multiple diseases in which astrocyte destruction is induced.[23]

The advent of mass spectrometry technologies have made it possible to uncover distinct molecular components associated with particular disease states.[20,24,25] However, as illustrated by the CSF-GFAP example above, similar changes of single components can be induced by multiple mechanisms. Hence, it may not be realistic to expect to find a single biomarker for complex disease processes that involve multiple underlying molecular mechanisms in their pathogenesis. Proteomic pattern analysis, a new method to search for biomarkers, is suitable for this purpose as it examines a panel of molecules; moreover, this approach can effectively distinguish seemingly closely-related diseases of a complex nature, such as MS-related disorders.

In this study, we analyzed CSF proteomic patterns from MS-related and non-MS control diseases by using magnetic bead-based enrichment of CSF peptides and proteins followed by matrix-assisted laser desorption/ionization time-of-flight (MALDI-TOF) mass spectrometry.[26] The current study reveals distinct CSF proteomic patterns between MS and anti-AQP4 antibody-defined disorder, confirmed by the 2 separated analysis with the same protocol but for different patient sets (which we have designated the first cohort and the second cohort). While the disorder characterized by LCL was found to have a proteomic pattern similar to the anti-AQP4 antibody-defined disorder in the first cohort, the result of the second cohort was inconsistent, indicating that this disorder have more than 1 proteomic pattern, and that the proteomic pattern is useful in classifying the disorders with LCL. We also succeeded in evaluating and visualizing the similarity of the proteomic pattern between neurological diseases analyzed.

Patients and Methods

Study Design

Patients were enrolled on the basis of clinical and laboratory features consistent with MS-related disorders. RRMS and PPMS subjects were diagnosed based on the revised McDonald criteria from 2005 (Polman and colleagues[27]). Patients seropositive for anti-AQP4 antibody were defined as seropositive NMOSD (SP-NMOSD), regardless of the distribution of their lesion. Seronegative NMOSD (SN-NMOSD) was applied to those who were seronegative for anti-AQP4 antibody and fit the McDonald MS criteria,[27] but exhibited LCL on spinal MRI.

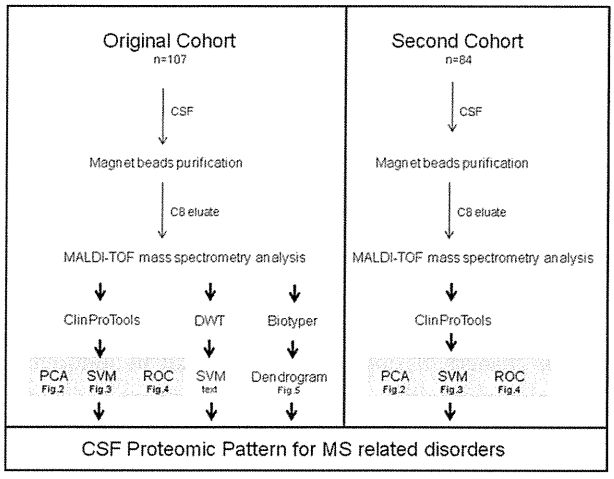

FIGURE 1: General workflow. This study was composed of 2 cohorts: the original one (n = 107) and the second one (n = 84). C8 = reversed phase column; DWT = discrete wavelet transformation; MALDI-TOF = matrix assisted laser desorption ionization–time of flight; PCA = principal component analysis, ROC = receiver operating characteristic curve; SVM = support vector machine.

Anti-AQP4 antibody was assayed in all patients with MS-related disorders. The assay was performed in a blinded manner (no patient information) by the standard method.[28] Patients with RRMS, SP-NMOSD, and SN-NMOSD were further divided among 2 clinical phases: relapse and remission. CSF samples from patients in the relapse phase were obtained prior to any treatment being administered to counter acute worsening, such as high-dose intravenous corticosteroid injection. The amyotrophic lateral sclerosis (ALS) group was considered as the control group and represented other degenerative neurological disease. The other inflammatory neurological disease (OIND) group was composed of patients suffering from aseptic encephalomeningitis (AEM), Guillain-Barr syndrome (GBS), and chronic inflammatory demyelinating polyneuropathy (CIDP). The second cohort study was also performed with the same protocol and it included RRMS, SP-NMOSD, SN-NMOSD, and OIND composed of AEM, GBS and CIDP.

The study protocol was approved by our ethics committee prior to enrolling patients, and all subjects provided written informed consent. The general workflow is illustrated in Figure 1.

Preparation of CSF samples for ClinProt Analysis

CSF samples were sent for routine diagnostics, including quantification of total protein, calculation of immunoglobulin G (IgG) index based on serum albumin and IgG concentration, and presence of oligoclonal IgG bands (OCB) as detected by isoelectric focusing and immunofixation. No sample contained more than 500 erythrocytes per microliter. All samples were centrifuged for 10 minutes at 3,000 rpm to separate the cellular elements for removal before storage at −80°C. Samples were prepared for analysis immediately upon thawing. A 5μl aliquot of the CSF was purified using magnetic beads with functionalized surface (hydrophobic interaction C8, MB-HIC 8; Bruker Daltonik GmbH, Bremen, Germany), according to the manufacturer's protocol. For mass spectrometric analysis, 1μl of the bead elute was mixed with 10μl of matrix solution (0.6g/liter a-cyano-4-hydroxycinnamic acid in 2:1 ethanol/acetone); 1μl of the mixture was then spotted in quadruplicate on a MALDI target MTP AnchorChip 600/384 (Bruker Daltonik GmbH).

Mass Spectrometry

Samples applied to the chip were analyzed on an Autoflex II MALDI-TOF mass spectrometer, operating in positive-ion linear mode (Bruker Daltonik GmbH). To generate a spectrum, 1,000 laser shots were acquired from random positions for each matrix spot. Four independent spectra were acquired for each spot. Acquisition was controlled by flexControl 3.0 software (Bruker Daltonik GmbH), using the AutoXecute tool and fuzzy control of laser intensity. The mass range analyzed was 1,000 to 15,000 mass to charge ratio (m/z). Spectra were externally calibrated using a mixture of standardized protein/peptide calibrants (ClinProt Standard, Bruker Daltonik GmbH).

Analysis of Proteomic Profile Spectra

The resulting spectra were analyzed using ClinProTools 2.2 bioinformatic software (Bruker Daltonik GmbH); the process included intensity normalization and spectral alignment using prominent internal peaks. As ClinProTools allows for discovery of discriminative peaks of spectra and can estimate how discriminative they are, we used the program to generate estimates of the respective potential for accurate diagnosis for each peak. Concomitant measures of specificity and sensitivity were also calculated. Peaks of interest were selected from the total average spectra, using a signal-to-noise threshold of 5.0. Finally, the ClinProTools was used to carry out comparative analysis of peak intensities between groups/disease classes, and to calculate corresponding statistics. When comparing 2 groups, we used analysis of variance (ANOVA) or the Wilcoxon-Mann-Whitney test. A cross-validation was performed on the same data by randomly assigning a group number to each CSF sample and then repeating the Wilcoxon-Mann-Whitney test.

Multivariate statistical analysis techniques, including principal component analysis (PCA)[29] and the support vector machine (SVM) algorithm (from ClinProTools), were employed to extract, display, and rank the variance within each data set. Through the calculation process of principal components (PCs), different weightings were assigned to each variable based on their contribution to the explained variance of a PC; in this manner, the contribution of single peaks to the variance covered by the respective PC was determined. To confirm the accuracy of SVM analysis, discrete wavelet transformation combined with SVM (DWT)[30] was employed.

We performed leave-1-out cross-validation (LOOCV) experiments using the SVM algorithm. In these analyses, different combinations of peptides selected by the Mann-Whitney U-test at different adjusted p value cutoffs were used to build the models and find significant peaks. The best models, ie, the

TABLE 1: Clinical and Laboratory Values for the First Cohort

	RRMS		SP-NMOSD		SN-NMOSD		PPMS	ALS	OIND
Clinical phase	Relapse	Remission	Relapse	Remission	Relapse	Remission			
Total patients	12	17	11	11	6	6	12	17	15
Male/female	6/6	6/11	3/8	0/11	0/6	0/6	4/8	13/4	11/4
Mean age at sampling, yr (range)	30 (17–40)	37 (16–57)	54 (33–64)	48 (17–81)	41 (37–60)	50 (38–58)	42 (32–51)	67 (44–72)	46 (15–62)
Disease duration, yr (range)	1.3 (0.1–17.3)	4.0 (0.3–27.3)	4.7 (0.3–8.1)	2.3 (0.2–10.0)	7.1 (1.4–10.0)	4.1 (0.5–19.0)	6.0 (0.5–20.0)	1.3 (0.1–10.0)	0.1 (0.0–1.3)
Average Expanded Disability Status Scale of Kurtzke (range)	2.3 (0.0–6.0)	1.0 (0.0–6.5)	7.5 (3.0–9.0)	5.0 (2.0–8.5)	8.0 (6.0–9.0)	8.3 (1.0–9.0)	4.5 (2.5–9.0)	n.e.	n.e.
Optic neuritis/total patients	5/12	4/17	9/11	8/11	5/6	4/6	0/12	n.e.	n.e.
Spinal MRI evidence of long cord lesions/total patients	0/12	0/17	11/11	9/11	6/6	6/6	0/12	n.e.	n.e.
Serum anti-AQP4 antibody positive/total patients	0/12	0/17	11/11	11/11	0/6	0/6	0/12	n.e.	n.e.
Fulfilling NMO criteria/total patients	0/12	0/17	9/11	7/11	5/6	4/6	0/12	n.e.	n.e.
CSF protein concentration, mg/dl (range)	36.0 (21.0–45.0)	30.0 (16.0–47.8)	60.0 (33.0–170.0)	30.1 (16.0–61.0)	65.1 (45.0–85.0)	33.0 (21.0–65.0)	39.5 (27.0–63.0)	35.8 (28.1–68.1)	54.8 (20.0–534.0)
IgG index, mg/dl (range)	0.67 (0.44–1.51)	0.61 (0.44–1.03)	0.62 (0.43–0.82)	0.53 (0.42–0.69)	0.57 (0.45–0.77)	0.49 (0.44–0.59)	0.87 (0.44–2.49)	0.49 (0.40–0.65)	0.65 (0.41–0.78)
Oligoclonal IgG bands/total patients	7/11	8/15	0/9	0/6	0/3	1/5	7/10	n.e.	n.e.

ALS = amyotrophic lateral sclerosis; AQP4 = aquaporin-4; CSF = cerebrospinal fluid; IgG = immunoglobulin G; MRI = magnetic resonance imaging; MS = multiple sclerosis; n.e. =; NMO = neuromyelitis optica; NMOSD = neuromyelitis optica spectrum disorder; OIND = other inflammatory neurological disease; PPMS = primary progressive MS; RRMS = relapsing-remitting MS; SN-NMOSD = anti-aquaporin4 antibody seronegative NMOSDO; SP-NMOSD = anti-aquaporin4 antibody seropositive NMOSD.

TABLE 2: Clinical and Laboratory Values for the Second Cohort

	RRMS		SP-NMOSD		SN-NMOSD		PPMS	ALS	OIND
Clinical phase	Relapse	Remission	Relapse	Remission	Relapse	Remission			
Total patients	15	15	4	7	2	5	2	18	16
Male/female	10/5	5/10	0/4	2/5	0/2	2/3	2/0	10/8	12/4
Mean age at sampling, yr (range)	39 (19–54)	43 (29–68)	47 (44–52)	48 (30–62)	48 (35–60)	48 (22–66)	58 (51–64)	62 (42–78)	48 (22–74)
Disease duration, yr (range)	4.4 (0.1–20.0)	5.3 (0.2–24.0)	2.3 (0.1–7.0)	1.2 (0.2–6.3)	3.3 (0.3–6.3)	7.1 (2.0–18.2)	7.9 (3.8–12.0)	2.2 (0.3–6.0)	0.9 (0.0–6.0)
Average Expanded Disability Status Scale of Kurtzke (range)	3.3 (2.0–6.5)	4.3 (1.0–7.5)	7.7 (7.5–8.0)	4.1 (1.0–7.0)	7.8 (7.5–8.0)	6.3 (6.0–6.5)	6.3 (5.5–7.0)	n.e.	n.e.
Optic neuritis/total patients	3/15	3/15	2/4	5/7	1/2	2/5	1/2	n.e.	n.e.
Spinal MRI evidence of long cord lesions/total patients	0/15	0/15	4/4	4/7	2/2	5/5	0/2	n.e.	n.e.
Serum anti-AQP4 antibody positive/total patients	0/15	0/15	4/4	7/7	0/2	0/5	0/2	n.e.	n.e.
CSF protein concentration, mg/dl (range)	36.6 (23.0–76.1)	36.4 (22.0–51.0)	86.7 (52.0–126.0)	39.7 (27.8–72.0)	58.0 (49.0–67.0)	44.0 (25.0–52.0)	29.8 (28.5–31.0)	41.7 (26.0–90.5)	81.5 (20.0–347.0)
IgG index, mg/dl (range)	0.89 (0.43–2.12)	0.54 (0.37–0.94)	0.70 (0.43–0.71)	0.47 (0.42–0.51)	0.55 (0.46–0.62)	0.52 (0.47–0.62)	0.59 (0.40–0.79)	0.51 (0.35–1.01)	0.56 (0.46–0.64)
Oligoclonal IgG bands/total patients	8/14	4/12	0/4	0/7	0/2	0/4	1/2	n.e.	n.e.

ALS = amyotrophic lateral sclerosis; AQP4 = aquaporin-4; CSF = cerebrospinal fluid; IgG = immunoglobulin G; MRI = magnetic resonance imaging; MS = multiple sclerosis; n.e. =; NMOSD = neuromyelitis optica spectrum disorder; OIND = other inflammatory neurological disease; PPMS = primary progressive MS; RRMS = relapsing-remitting MS; SN-NMOSD = anti-aquaporin4 antibody seronegative NMOSDO; SP-NMOSD = anti-aquaporin4 antibody seropositive NMOSD.

ones giving the smaller classification error rate in the cross-validation of the first cohort, were tested. We then examined an independent collection of 84 CSF samples as a second cohort and replicated the above mentioned calculation as shown in Figure 1.

Pattern Matching of the CSF Proteomic Spectra

We applied the MALDI Biotyper algorithm (Bruker Daltonik GmbH)[31,32] to the spectra obtained from the CSF samples, according to the manufacturer's protocols. For phylogenetic analysis, we hierarchically clustered mass spectra corresponding to each disease group. For graphical correlations, an average statistical algorithm was implemented in the MALDI Biotyper software. Reference spectra were analyzed and compared for the nine disease stages (ALS, PPMS, RRMS remission, RRMS relapse, OIND, SP-NMOSD remission, SP-NMOSD relapse, SN-NMOSD remission, and SN-NMOSD relapse). Based on the distance values obtained, a list of mass signals and their intensities was taken into consideration, and a dendrogram was produced by a similar scoring method using a set of mass spectra to determine distance values between disease groups. According to previous analogous bacterial identification experiments for group-by-group comparisons,[31] distance levels <500 were considered to indicate "reliable similar classification." We applied this standard of distance values to our evaluation of the similarity of CSF protein patterns.

Results

Subject and CSF Characteristics of the First and the Second Cohort

We analyzed 107 CSF samples from patients diagnosed with RRMS (n = 29), SP-NMOSD (n = 22), SN-NMOSD (n = 12), PPMS (n = 12), ALS (n = 17), and OIND (n = 15). The OIND group was composed of patients suffering from AEM (n = 7), GBS (n = 4), and CIDP (n = 4). Clinical information, including routine CSF and MRI findings, are summarized in Table 1. Of the 22 SP-NMOSD patients, 16 (72.7%) fulfilled the 2006 Mayo NMO criteria,[4] as did 9 of the 12 (75.0%) SN-NMOSD patients. The remaining 6 individuals with SP-NMOSD and 3 with SN-NMOSD lacked detectable optic nerve lesions or spinal lesions.

We put 84 CSF samples from patients diagnosed with RRMS (n = 30), SP-NMOSD (n = 11), SN-NMOSD (n = 7), PPMS (n = 2), ALS (n = 18), and OIND (n = 16) as the second cohort. OIND includes 8 CIDP, 4 GBS, and 4 AEM. Clinical information of these patients is summarized in Table 2.

Discrimination Among MS-Related Disorders by PCA

In the mass range analyzed (m/z 1,000–15,000), an average of 108 peaks per subset spectrum were detected at a signal-to-noise threshold of 5.0 (Supplementary Figure 1). The loading coefficients were found to indicate that more than 50 peaks predominantly contributed to the separation of RRMS relapse and SP-NMOSD relapse groups (Supplementary Figure 2).

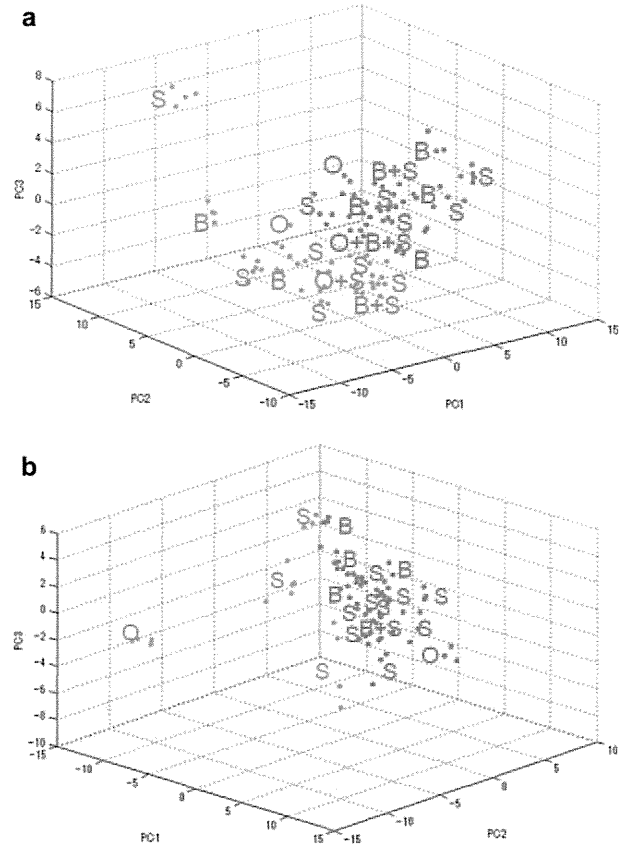

FIGURE 2: Representation of the principal components (PCs) generation from a data set. For each CSF sample, 4 measurements were automatically performed and represented a combination of clinically manifested CNS lesion sites. O = optic nerve; S = spinal cord; B = brain. (A) Principal component analysis (PCA) score plot indicating that RRMS relapse patients (*red*) clustered separately from SP-NMOSD relapse patients (*green*) based on the first cohort. (B) PCA score plot indicating that RRMS relapse patients (*red*) clustered separately from SP-NMOSD relapse patients (*green*) based on the second cohort.

Comparative analysis of spectra between disease groups revealed a number of peaks with significant differences in intensity. PCA showed that discrimination between each disease category was distinct. For example, RRMS relapse and SP-NMOSD relapse was clearly discriminated by PCA (Fig 2A). This result is also replicated by the second cohort (see Fig 2B). Furthermore, distribution of CNS lesions do not have significant power on proteomic pattern discrimination.

One can argue a possibility that difference in the sex ratio, age, disease severity, presence or absence of OCB, or distribution of CNS lesions have significant power on proteomic patterns. To address this question, the PCA analysis was carried. The results statistically and

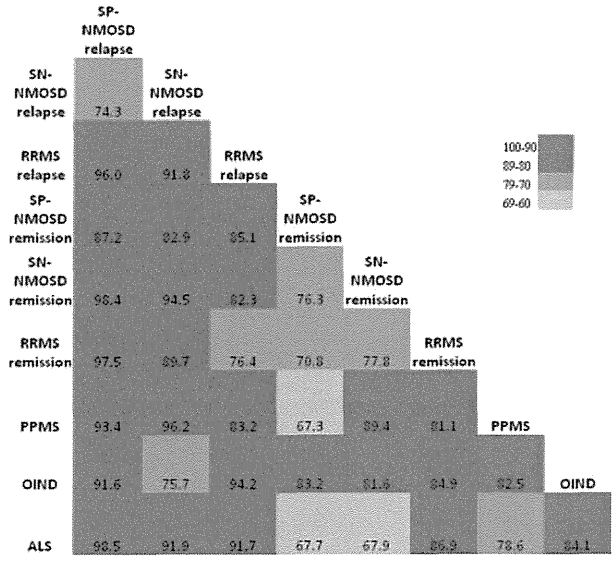

FIGURE 3: Heat map of the SVM analysis to differentiate patients with SP-NMOSD, SN-NMOSD, RRMS, PPMS, OIND, and ALS. Cross-validation analysis provided an estimate of the success rate for the SVM model to separate user-defined groups of spectra. RRMS and SP-NMOSD were well-separated by SVM. The distinct proteomic profiles of RRMS and SP-NMOSD were confirmed in relapse phase and, to a lesser extent, in the remission phase. The variation of proteomic profiles between relapse and remission phases was robust for SP-NMOSD, but less so for RRMS. The *x*-axis and *y*-axis represent the samples, ordered by group. The accuracy is denoted by color: 90% to 100% (*red*); 80% to 89% (*pink*); 70% to 79% (*purple*); and 60% to 69% (*blue*) (see inset key).

reproducibly showed that each of the above differences had little impact on distinction of proteomic patterns of relevant diseases (Supplementary Figure 3A and B).

Discrimination Among MS-Related Disorders by SVM

To automatically detect differences of the obtained spectra at different disease stages, we applied a supervised model generation procedure in combination with SVM, an approach based on machine learning. Cross-validation analysis provided an estimate of the success rate for the SVM model to separate user-defined groups of spectra (Fig 3). For example, SVM analysis between RRMS remission and OIND resulted in cross-validation accuracy of 84.9%; between RRMS relapse and OIND, accuracy was determined to be 94.2%. The RRMS and SP-NMOSD groups were well separated by SVM (96.0%, RRMS relapse vs SP-NMOSD relapse; 70.8%, RRMS remission vs SP-NMOSD remission). Therefore, this method was able to confirm that patients with RRMS and SP-NMOSD exhibited distinct proteomic profiles in the relapse phase, and to a lesser extent in the remission phase. The change of proteomic profiles that occurred between relapse and remission phases was found to be more prominent in SP-NMOSD, and less so in RRMS. SVM cross-validation accuracies were 76.4% for RRMS and 87.2% for SP-NMOSD. SVM analysis between RRMS remission and PPMS yielded an accuracy rate of 81.1%; moreover, SVM between RRMS relapse and PPMS had an accuracy of 83.2%. RRMS and SN-NMOSD showed distinct features (91.8%, RRMS relapse vs SN-NMOSD relapse; 77.8%, RRMS remission vs SN-NMOSD remission). SVM analyses between SP-NMOSD and SN-NMOSD were found to have an

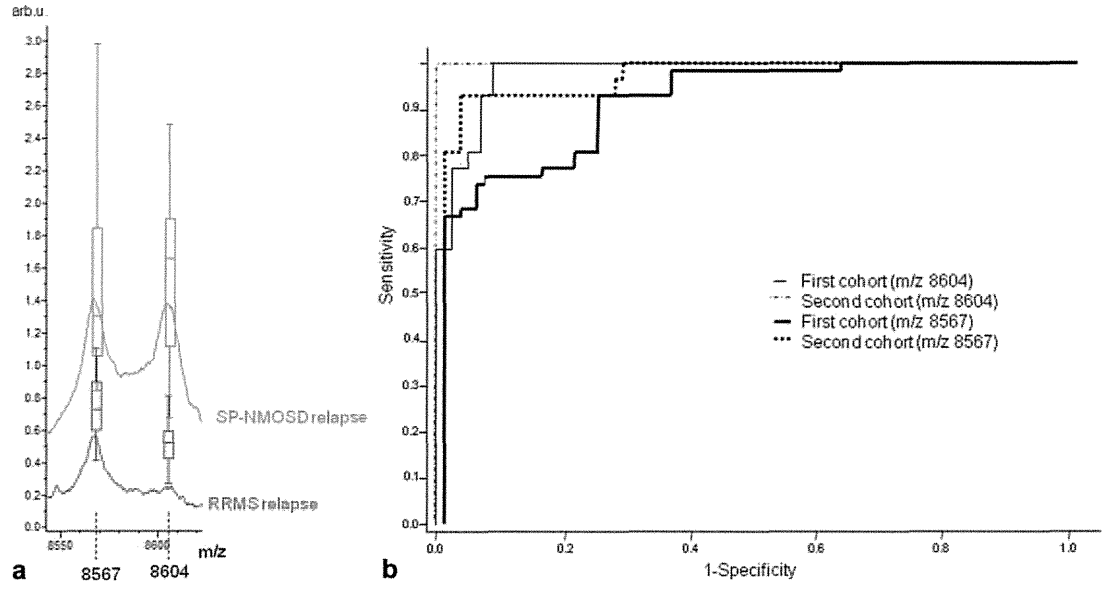

FIGURE 4: Analysis by receiver operating characteristic curves. (A) Average spectral features and box-and-whisker plots at m/z 8567 and 8604, representative markers for RRMS vs SP-NMOSD in relapse phase. SP-NMOSD relapse (*green*); RRMS relapse (*red*). The *x*-axis and *y*-axis represent the relative intensity and m/z, respectively. (B) Changes in key markers of RRMS relapse and SP-NMOSD relapse were validated by ROC curve of m/z 8567 and 8604.

TABLE 3: AUC Determined by ROC Analysis for Each Peak Used in the Cluster to Differentiate RRMS and SP-NMOSD/SN-NMOSD Relapse Phases

m/z	RRMS relapse vs SP-NMOSD relapse[a]	RRMS relapse vs SN-NMOSD relapse[a]
8604	0.996/1	0.991/0.810
6970	0.980/0.884	0.990/0719
4644	0.970/0.617	0.979/0.559
8567	0.957/0.979	0.976/0.734
7033	0.950/0.810	0.956/0.542

[a]Values are given as first cohort/second cohort.AUC = area under the ROC curve; m/z = mass to charge ratio; NMOSD = neuromyelitis optica spectrum disorder; ROC = receiver operating characteristic; RRMS = relapsing remitting multiple sclerosis; SN-NMOSD = anti-aquaporin4 antibody seronegative NMOSD; SP-NMOSD = anti-aquaporin4 antibody seropositive NMOSD.

accuracy of 74.3% in relapse and 76.3% in remission. DWT emphasized the distinction between RRMS and SP-NMOSD in relapse stages, with 86.5% double cross-validation accuracy. These observations are well validated by the second cohort as shown in Supplementary Figure 4.

Analysis by Receiver Operating Characteristics Curves

The sensitivity and specificity of each peak was calculated by the receiver operating characteristics (ROC) analysis (Fig 4A, B; Table 3). Each of the peaks showed high accuracy in discriminating RRMS from SP-NMOSD in relapse phases, by using the area under the ROC curve (AUC). The areas of these peaks in the spectra were found to be statistically different. Moreover, 5 of these peaks had AUC > 0.95 when RRMS relapse was compared with SP-NMOSD relapse. This analysis was even better replicated by the second cohort (see Fig 4B). In Table.3, while discrimination between RRMS relapse and the SP-NMOSD relapse phase was well validated by the first and second cohort, discrimination between RRMS relapse and SN-NMOSD was not replicated. In Supplementary Figure 5A and 5B, this situation is visualized by 2D distribution view of 2 selected peaks, x = 8604 and y = 8567 in the spectrum of loaded model generation classes.

"Pattern Matching" Spectral Differences Among Reference Disease Groups

Using the MALDI Biotyper 2.0 software, 9 reference disease groups were analyzed and their similarities were visualized in a dendrogram (Fig 5). The CSF proteomic patterns of disease were clearly divided into 3 main groups with distance values >500. One group was composed of RRMS, PPMS, and ALS, while a second group included SP-NMOSD, SN-NMOSD, and OIND. Except for the comparison between SP-NMOSD and SN-NMOSD, the distance values of proteomic patterns between relapse and remission phases for the same disorder were shorter than that in comparison to different disease groups. The distance value of proteomic patterns between the remission phases of SP-NMOSD and SN-NMOSD was 88, but the distance value increased to 446 for the relapse phases; this finding indicated that the

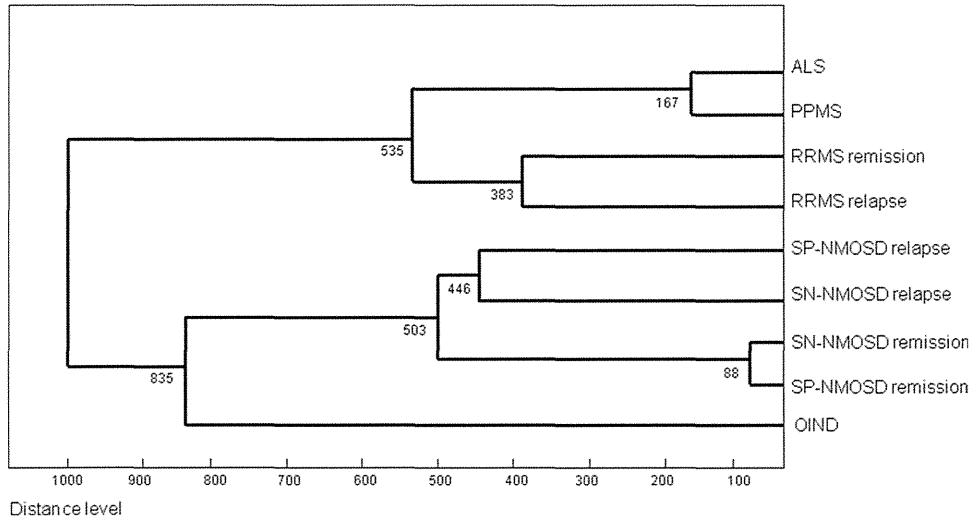

FIGURE 5: Score-oriented dendrogram of MALDI-TOF mass spectral profiles generated by the MALDI Biotyper. Reference spectra were generated for each of 9 different disease groups. Similarity was visualized by a rooted tree. The distance level is presented as percentage.

patterns still resembled each other at relapse, but the differences were clearer than in remission stages. Surprisingly, PPMS, RRMS, and ALS classified with the same group. The distance values of proteomic patterns between PPMS and ALS was 167, and distinctly shorter than that of PPMS and any of the other inflammatory diseases, including SP-NMOSD and SN-NMOSD.

Discussion

In this study, we demonstrated that CSF proteomic patterns can effectively discriminate MS from other MS-related disorders. Proteomic profiles of CSF from the relapse phase of SP-NMOSD and SN-NMOSD are distinct from those of RRMS. As there is a strong need to develop therapeutic guidelines specific to each of the MS-related disorders, detection of process-specific biomarkers represents an important new direction toward this end. As we have shown here, CSF proteomic pattern analysis could afford clinicians the possibility to make clear distinctions among MS-related disorders that are much less influenced by the size and distribution of disease lesions. CSF sampling without trypsin digestion presents an advantage in analyzing the native CSF proteome, thus potentially allowing for the direct measurement of enzymatically cleaved proteins of pathological relevance.[20]

SVM, a mathematical algorithm based on supervised learning methods, has proven to be a useful tool to detect differences between created models, especially when small datasets are applied. To confirm the accuracy of SVM in this study, in a completely different approach of spectral processing we employed DWT, which is a specific kind of Fourier transformation. This method is also considered to be superior in treating relatively small number of samples. In the relapse phase of RRMS and SP-NMOSD, discrimination of each disease by CSF proteomic profiling was much easier to accomplish than in the remission phase, indicating that dynamic autodestructive processes may be reflected in the CSF proteomic profiles.

SN-NMOSD and SP-NMOSD have only recently be recognized as components of the NMO-spectrum.[2] However, controversy exists as to where SN-NMOSD should be classified between RRMS and SP-NMOSD. Hence, the rational selection of therapy for SN-NMOSD remains unclear. In the first cohort, 5 common discriminative mass spectra peaks with high AUC scores (>0.95) between SN-NMOSD and SP-NMOSD were found to be discriminative between the 2 NMO-spectrum disorders and RRMS in relapse phases. We believe from this result that most of SN-NMOSD has similar or identical pathogenesis to SP-NMOSD. However, the 2 samples with SN-NMOSD in the second cohort have a different pattern (see Table 3; Supplementary Figure 5A and B). There is little possibility that the difference was due to a methodological error since the reproducibility was quite robust for the other disorders in analysis. It is more likely that SN-NMOSD have more than 1 population with distinct pathogenesis. Indeed, LCL findings in MRI can admit more than 1 condition. Adjacent spinal lesions in advanced stage of MS can be indistinguishable to a single continuous long lesion in the MRI study. The result may show that proteomic pattern can be a strong tool for clarifying multiple disorders not easy to separate by conventional methods.

The MALDI Biotyper was developed as a mass spectrometry-based platform for identification and classification of microorganisms.[31] The patterns of protein masses observed by MALDI-mass spectrometry have been successfully used for accurate classification and identification of bacteria. In this study, we have applied the MALDI Biotyper software solution for discriminating proteomic patterns in human neurological disease. To our surprise, the resulting dendrogram was composed of 3 major "islands." ALS and PPMS were classified as the disease entities nearest to RRMS, with relapse and remission stages composing the first island. These disease entities were clearly discriminated from SP-NMOSD and SN-NMOSD, with relapse and remission stages composing the second island on the dendrogram. OIND, which included disorders with a prominent CNS inflammatory feature, produced the third island, which was closer to the second island of SP-NMOSD and SN-NMOSD. The finding that PPMS was situated next to ALS may indicate that the CSF proteomic patterns for PPMS and ALS represent less inflammation or merely a small skew from the normal state. However, recent reports have suggested another possibility in that PPMS has more neurodegenerative features than other MS-related disorders.[13,33,34] Alternatively the observation here may support involvement of the immune system in ALS to mediate either neurotoxicity or neuroprotection events.[35] These are open questions that will likely be answered in future studies.

MRI evidence of LCL is currently considered the most characteristic feature of NMO,[4] and is indispensable for NMO diagnosis. However, early therapeutic intervention can prevent the extension of spinal cord lesions. In this situation, tracking of disease progress can be impeded by the relative stabilization of lesions. Our procedure is not influenced by size and distribution of lesions, and will provide more solid information to

differentiate among MS-related diseases, especially for SP-NMOSD/SN-NMOSD.

In conclusion, our applied proteomic pattern analysis facilitated the effective distinction of similar MS-related disorders, and revealed a possibility that these patterns, themselves, can be used as biomarkers for each disorder.

Acknowledgments

We thank Dr. Keiko Tanaka for analysis of the serum anti aquaporin-4 antibody in patient samples and Etsuko Nishiguchi for assistance in treating CSF samples. We also acknowledge Atsuhiro Kanzaki for excellent assistance in our statistical analysis.

References

1. Sospedra M, Martin R. Immunology of multiple sclerosis. Annu Rev Immunol 2005;23:683–747.
2. Wingerchuk DM, Lennon VA, Lucchinetti CF, et al. The spectrum of neuromyelitis optica. Lancet Neurol 2007;6:805–815.
3. Tanaka M, Tanaka K, Komori M. Interferon-beta(1b) treatment in neuromyelitis optica. Eur Neurol 2009;62:167–170.
4. Wingerchuk DM, Lennon VA, Pittock SJ, et al. Revised diagnostic criteria for neuromyelitis optica. Neurology 2006;66:1485–1489.
5. Lennon VA, Wingerchuk DM, Kryzer TJ, et al. A serum autoantibody marker of neuromyelitis optica: distinction from multiple sclerosis. Lancet 2004;364:2106–2112.
6. Lennon VA, Kryzer TJ, Pittock SJ, et al. IgG marker of optic-spinal multiple sclerosis binds to the aquaporin-4 water channel. J Exp Med 2005;202:473–477.
7. Tanaka M, Tanaka K, Komori M, Saida T. Anti-aquaporin 4 antibody in Japanese multiple sclerosis: the presence of optic spinal multiple sclerosis without long spinal cord lesions and anti-aquaporin 4 antibody. J Neurol Neurosurg Psychiatry 2007;78: 990–992.
8. Pittock SJ, Weinshenker BG, Lucchinetti CF, et al. Neuromyelitis optica brain lesions localized at sites of high aquaporin 4 expression. Arch Neurol 2006;63:964–968.
9. McKeon A, Fryer JP, Apiwattanakul M, et al. Diagnosis of neuromyelitis spectrum disorders: comparative sensitivities and specificities of immunohistochemical and immunoprecipitation assays. Arch Neurol 2009;66:1134–1138.
10. Cabrera-Gomez JA, Bonnan M, Gonzalez-Quevedo A, et al. Neuromyelitis optica positive antibodies confer a worse course in relapsing-neuromyelitis optica in Cuba and French West Indies. Mult Scler 2009;15:828–833.
11. Miller DH, Leary SM. Primary-progressive multiple sclerosis. Lancet Neurol 2007;6:903–912.
12. Koch M, Kingwell E, Rieckmann P, Tremlett H. The natural history of primary progressive multiple sclerosis. Neurology 2009;73: 1996–2002.
13. Frischer JM, Bramow S, Dal-Bianco A, et al. The relation between inflammation and neurodegeneration in multiple sclerosis brains. Brain 2009;132:1175–1189.
14. Hammack BN, Fung KY, Hunsucker SW, et al. Proteomic analysis of multiple sclerosis cerebrospinal fluid. Mult Scler 2004;10: 245–260.
15. Noben JP, Dumont D, Kwasnikowska N, et al. Lumbar cerebrospinal fluid proteome in multiple sclerosis: characterization by ultrafiltration, liquid chromatography, and mass spectrometry. J Proteome Res 2006;5:1647–1657.
16. Stoop MP, Dekker LJ, Titulaer MK, et al. Quantitative matrix-assisted laser desorption ionization-Fourier transform ion cyclotron resonance (MALDI-FT-ICR) peptide profiling and identification of multiple-sclerosis-related proteins. J Proteome Res 2009;8: 1404–1414.
17. Dumont D, Noben JP, Raus J, et al. Proteomic analysis of cerebrospinal fluid from multiple sclerosis patients. Proteomics 2004;4: 2117–2124.
18. Lehmensiek V, Sussmuth SD, Tauscher G, et al. Cerebrospinal fluid proteome profile in multiple sclerosis. Mult Scler 2007;13:840–849.
19. D'Aguanno S, Barassi A, Lupisella S, et al. Differential cerebro spinal fluid proteome investigation of Leber hereditary optic neuropathy (LHON) and multiple sclerosis. J Neuroimmunol 2008;193: 156–160.
20. Irani DN, Anderson C, Gundry R, et al. Cleavage of cystatin C in the cerebrospinal fluid of patients with multiple sclerosis. Ann Neurol 2006;59:237–247.
21. Ottervald J, Franzén B, Nilsson K, et al. Multiple sclerosis: Identification and clinical evaluation of novel CSF biomarkers. J Proteomics 2010;73:1117–1132.
22. Comabella M, Fernandez M, Martin R. et al. Cerebrospinal fluid chitinase 3-like 1 levels are associated with conversion to multiple sclerosis. Brain 2010;133:1082–1093.
23. Misu T, Takano R, Fujihara K, et al. Marked increase in cerebrospinal fluid glial fibrillar acidic protein in neuromyelitis optica: an astrocytic damage marker. J Neurol Neurosurg Psychiatry 2009; 80:575–577.
24. Pasinetti GM, Ungar LH, Lange DJ, et al. Identification of potential CSF biomarkers in ALS. Neurology 2006;66:1218–1222.
25. Huang JT, Leweke FM, Oxley D, et al. Disease biomarkers in cerebrospinal fluid of patients with first-onset psychosis. PLoS Med. 2006;3:e428.
26. Sekiyama E, Matsuyama Y, Higo D, et al. Applying magnetic bead separation/MALDI-TOF mass spectrometry to human tear fluid proteome analysis. J Proteomics Bioinform 2008;1:368–373.
27. Polman CH, Reingold SC, Edan G, et al. Diagnostic criteria for multiple sclerosis: 2005 revisions to the "McDonald Criteria." Ann Neurol 2005;58:840–846.
28. Tanaka K, Tani T, Tanaka M, et al. Anti-aquaporin 4 antibody in selected Japanese multiple sclerosis patients with long spinal cord lesions. Mult Scler 2007;13:850–855.
29. Ivosev G, Burton L, Bonner R. Dimensionality reduction and visualization in principal component analysis. Anal Chem 2008;80: 4933–4944.
30. Alexandrov T, Decker J, Mertens B, et al. Biomarker discovery in MALDI-TOF serum protein profiles using discrete wavelet transformation. Bioinformatics 2009;25:643–649.
31. Freiwald A, Sauer S. Phylogenetic classification and identification of bacteria by mass spectrometry. Nat Protoc 2009;4:732–742.
32. Nagy E, Maier T, Urban E, et al. Species identification of clinical isolates of Bacteroides by matrix-assisted laser-desorption/ionization time-of-flight mass spectrometry. Clin Microbiol Infect 2009; 15:796–802.
33. Leray E, Yaouanq J, Le Page E, et al. Evidence for a two-stage disability progression in multiple sclerosis. Brain 2010;133: 1900–1913.
34. Tallantyre EC, Bo L, Al-Rawashdeh O, et al. Greater loss of axons in primary progressive multiple sclerosis plaques compared to secondary progressive disease. Brain 2009;132:1190–1199.
35. Appel SH, Beers DR, Henkel JS. T cell-microglial dialogue in Parkinson's disease and amyotrophic lateral sclerosis: are we listening? Trends Immunol 2010;31:7–17.

RESEARCH ARTICLE

Cerebrospinal Fluid Proteomic Patterns Discriminate Parkinson's Disease and Multiple System Atrophy

Noriko Ishigami, MD,[1] Takahiko Tokuda, MD, PhD,[1,2] Masaya Ikegawa, MD, PhD,[3]* Mika Komori, MD, PhD,[4] Takashi Kasai, MD, PhD,[1] Takayuki Kondo, MD, PhD,[5] Yumiko Matsuyama, PhD,[6] Takashi Nirasawa, PhD,[6] Herbert Thiele, PhD,[7] Kei Tashiro, MD, PhD,[3] and Masanori Nakagawa, MD, PhD[1]

[1]*Department of Neurology, Kyoto Prefectural University of Medicine, Kamigyo-ku, Kyoto, Japan*
[2]*Department of Molecular Pathobiology of Brain Diseases, Kyoto Prefectural University of Medicine, Kamigyo-ku, Kyoto, Japan*
[3]*Department of Genomic Medical Sciences, Kyoto Prefectural University of Medicine, Kamigyo-ku, Kyoto, Japan*
[4]*Department of Neurology, Graduate School of Medicine, Kyoto University, Shogoin, Sakyo-ku, Kyoto, Japan*
[5]*Department of Neurology, Tazuke Kofukai Medical Research Institute and Kitano Hospital, Kita-ku, Osaka, Japan*
[6]*Bruker Daltonics K.K., Yokohama, Kanagawa, Japan*
[7]*Bruker Daltonik GmbH., Bremen, Germany*

ABSTRACT: The differential diagnosis of Parkinson's disease and multiple system atrophy can be challenging, especially in the early stages of the diseases. We developed a proteomic profiling strategy for parkinsonian diseases using mass spectrometry analysis for magnetic-bead-based enrichment of cerebrospinal fluid peptides/proteins and subsequent multivariate statistical analysis. Cerebrospinal fluid was obtained from 37 patients diagnosed with Parkinson's disease, 32 patients diagnosed with multiple system atrophy, and 26 patients diagnosed with other neurological diseases as controls. The samples were from the first cohort and the second cohort. Cerebrospinal fluid peptides/proteins were purified with C8 magnetic beads, and spectra were obtained by matrix-assisted laser desorption ionization time-of-flight mass spectrometry. Principal component analysis and support vector machine methods are used to reduce dimension of the data and select features to classify diseases. Cerebrospinal fluid proteomic profiles of Parkinson's disease, multiple system atrophy, and control were differentiated from each other by principal component analysis. By building a support vector machine classifier, 3 groups were classified effectively with good cross-validation accuracy. The model accuracy was well preserved for both cases, training by the first cohort and validated by the second cohort and vice versa. Receiver operating characteristics proved that the peak of *m/z* 6250 was the most important to differentiate multiple system atrophy from Parkinson's disease, especially in the early stages of the disease. A proteomic pattern classification method can increase the accuracy of clinical diagnosis of Parkinson's disease and multiple system atrophy, especially in the early stages. © 2012 *Movement* Disorder Society

Key Words: Parkinson's disease; multiple system atrophy; proteomics; cerebrospinal fluid; biomarkers

Parkinson's disease (PD) is the second most common neurodegenerative disorder, increasing in prevalence with age.[1] Multiple system atrophy (MSA) is a rare atypical parkinsonian disorder and has a relatively poor prognosis compared with PD because of much more widespread neurodegeneration.[2] The diagnoses of PD and MSA are still based on clinical features,[1–4] and differential diagnosis may be challenging, especially in the early-disease stages.[1] The development of reliable biochemical markers would have profound implications for clinical management and basic research.

By its direct communication with the extracellular fluid surrounding brain cells, cerebrospinal fluid (CSF) directly reflects the metabolic and pathological status of the central nervous system and is an ideal source for biochemical markers for parkinsonian disorders.

Noriko Ishigami and Takahiko Tokuda contributed equally to this work.

***Correspondence to:** Dr. Masaya Ikegawa, Department of Genomic Medical Sciences, Kyoto Perfectural University of Medicine, 465 Kajii-cho, Kamigyo-ku, Kyoto 602-8566, Japan; mikegawa@koto.kpu-m.ac.jp

Relevant conflicts of interest/financial disclosures: Nothing to report. Full financial disclosures and author roles may be found in the online version of this article.

Received: 20 June 2011; **Revised:** 27 February 2012; **Accepted:** 9 March 2012
Published online 1 June 2012 in Wiley Online Library (wileyonlinelibrary.com). DOI: 10.1002/mds.24994

Although previous studies have shown differences in the levels of certain CSF proteins such as α-synuclein and DJ-1 between patients with PD and those with other forms of parkinsonism, their potential as differentiating biomarkers for these diseases has not yet been validated.[5–8] It may not be realistic to expect to find a single biomarker for complex disease processes involving multiple underlying molecular mechanisms of pathogenic importance. With emerging state-of-the-art technology,[9–13] proteomic pattern analysis, a new method to search for biomarkers, is suitable for this purpose, as it examines a panel of molecules; moreover, this approach can effectively distinguish apparently closely related diseases of a complex nature by computational statistical methods.[14]

In the current study, we asked whether the CSF proteomic profile analyzed by the ClinProt protocol (Bruker Daltonik GmbH) could classify PD, MSA, and controls.[12,13] Various statistical and machine-learning methods have been used to analyze the high-dimensional data generated by mass spectrometry.[14] Principal component analysis (PCA) is an unsupervised dimension reduction method generating orthogonal projections of the data, which is useful to highlight distinctive patterns in multivariate data. In contrast, support vector machine (SVM) is a powerful supervised machine-learning method for classification and pattern recognition. Here we have demonstrated the suitability of the SVM classifier in the CSF proteome when trained in the first cohort to classify the samples in the second cohort and demonstrated the suitability when trained in the second cohort to classify the samples in the first cohort. Furthermore, we evaluated classification performance of the SVM by considering the area under the receiver operating characteristics (ROC) curve, and the most optimal mass was nominated for the classification of PD and MSA.

Our findings suggest that CSF proteomic pattern analysis can increase the accuracy of disease diagnosis of PD-related disorders and may ultimately aid physicians in appropriate therapeutic decision making.

Patients and Methods

Subjects

We enrolled 26 patients with clinically defined PD and 23 patients with probable and possible MSA as the first cohort (Table 1). These subjects were recruited from the Department of Neurology, Kyoto Prefectural University Hospital, Kyoto, Japan, between April 2002 and February 2009. The patients with PD or MSA were diagnosed according to the United Kingdom Parkinson's Disease Society Brain Bank clinical diagnostic criteria[1] and the second consensus criteria for MSA,[3] respectively. Clinical data were retrieved from patient charts and confirmed by 3 board-certified neurologists. We defined the patients with PD and MSA who were examined fewer than 3 years after onset as the patients in the early stage of the disease. The 26 age-matched control subjects (Table 1) in the first cohort were neurologically normal individuals who underwent lumbar puncture as part of the diagnostic process (n = 13), and controls with various neurologic disorders without involvement of the brain (n = 13), including patients with peripheral neuropathy (n = 6), myelopathy (n = 3), epilepsy (n = 3), and myopathy (n = 1).

TABLE 1. Patient demographics and clinical data from the first and second cohorts

Diagnosis	Number of cases	Sex (F/M)	Mean age (± SD) at LP (y)	Duration of disease (n)	
				<3 years	≥3 years
First cohort					
PD (total)	26	11/15	66.3 ± 11.2	13	13
H&Y 1–2	11	5/6	69.5 ± 11.8	7	4
H&Y 3–4	15	6/9	63.9 ± 10.5	6	9
MSA (total)	23	6/17	62.4 ± 7.5	15	8
Probable	7	2/5	60.6 ± 8.5	4	3
Possible	16	4/12	63.2 ± 7.1	11	5
Controls	26	12/14	63.4 ± 12.4	—	—
Second cohort					
PD (total)	11	4/7	64.6 ± 11.7	—	—
MSA (total)	9	5/4	56.1 ± 7.7	—	—

Abbreviations: PD, Parkinson's disease; MSA, multiple system atrophy; H&Y, Hoehn and Yahr stage; LP, lumbar puncture.

The second cohort, which was collected for validation, included 11 clinically defined PD patients whose CSF samples were collected and stored between January 2005 and January 2010 and 9 age-matched MSA patients whose CSF samples were taken and stored between January 1995 and January 2001 (Table 1). Both groups of patients were diagnosed according to the same clinical criteria applied to the first cohort. The diagnosis of each patient was concealed prior to experiments to facilitate blind testing.

All the study subjects provided written informed consent to participate, which was approved by the university ethics committee (Kyoto Prefectural University, Kyoto, Japan). The study procedures were designed and performed in accordance with the Declaration of Helsinki.

Collection and Preparation of CSF Samples

The collected CSF samples were gently mixed to avoid gradient effects, then stored at −80°C. A 20-μL aliquot of the CSF samples was subjected to SDS-PAGE followed by CBB staining to ensure that no samples were contaminated with hemoglobin (data not shown). A 5-μL aliquot of the CSF from each subject was purified using magnetic beads with a functionalized surface (hydrophobic C8-coated magnetic

beads, MB-HIC, Bruker Daltonik GmbH, Bremen, Germany) according to the manufacturer's protocol. For MS analysis, 1 μL of bead eluate was mixed with 10 μL of matrix solution (0.6 g/L α-cyano-4-hydroxycinnamic acid in 2:1 ethanol/acetone), and 1 μL of the mixture was then spotted in quadruplicate on a MALDI target MTP AnchorChip 600/384 (Bruker Daltonik GmbH, Bremen, Germany).

Mass Spectrometry

Samples applied to the AnchorChip were analyzed on an autoflex MALDI-TOF mass spectrometer (Bruker Daltonik GmbH, Bremen, Germany) operating in positive-ion linear mode. To generate a spectrum, 1000 laser shots were acquired from random positions for each matrix spot. Four independent spectra were acquired for each spot. Acquisition was controlled by flexControl 3.0 software (Bruker Daltonik GmbH, Bremen, Germany) using the AutoXecute (Bruker Daltonik GmbH), and fuzzy control of laser intensity. The mass range analyzed was 1000–15,000 *m/z* at a signal-to-noise threshold of 5. Spectra were externally calibrated using a mixture of standardized protein/peptide calibrants (ClinProt Standard, Bruker Daltnik GmbH, Bremen, Germany). The same MS analysis was replicated 3 times on different experimental days.

Analysis of Proteomic Profiles

The resulting spectra were analyzed using ClinProTools 2.2 bioinformatic software (Bruker Daltonik GmbH, Bremen, Germany).[12] Peaks of interest were selected from the total average spectra, using a signal-to-noise threshold of 5. Data normalization was performed as (1) spectra normalization to the total ion current; (2) spectra recalibration using the prominent peaks; (3) baseline subtraction, smoothing, and peak detection; and (4) calculation of peak areas for each spectrum. First, PCA was employed to visualize the distribution of the data.[15] The feature selections of PCA are present in the top principal components (PCs), which separate the samples into homogeneous clusters and can be visualized in 3-D plots in which the calculated values for top PCs serve as *x*, *y*, and *z* axes.[14] The loading plots, which are the variance plots, show how PCs are related to the original peaks. An SVM, another machine-learning approach, was applied to the current mass data for selection of clusters of signals able to discriminate the 2 objective groups.[12] Cross-validation accuracy is the percentage of data correctly classified. To test the classifier accuracy, the training data set and the testing data set were tested vice versa. Finally, ROC analysis for each peak of interest was performed, and the area under the curve (AUC) score was plotted for each selected feature.[14]

Results

Principal Component Analysis for the First and Combined Cohort Data Sets

PCA scores plotted based on MALDI spectra of CSF samples showed a clear difference between MSA and control (Fig. 1C) and a probable difference between PD and control (Fig. 1A) in the first cohort samples. To our surprise, if we replicated this for the first and second cohorts combined, it showed extremely good separation between PD and control (Fig. 1B) and between MSA and control (data not shown). These data indicate that PD and MSA are quite different from the control in terms of CSF proteomic pattern. Between PD versus MSA, compared with the above-described comparisons, the differentiation was a bit decreased. However, in analyzing the second cohort, very good separation was observed. When we compared the early parkinsonian subsets, it also showed good separation. The PCA loadings plot, which provided information about the contribution of single peaks to the variance covered by the respective PC, demonstrated that no single peak significantly contributed to the variance, but many peaks contributed to discrimination between PD and control, between MSA and control, and between PD and MSA (data not shown).

SVM Model for the First and Second Cohorts

For further evaluation of experiment-to-experiment data stability, we performed mass data analysis on 3 different experimental days using the same sample sets (Table 2). Cross-validation analysis provided an estimate of the reliability of the SVM model to classify defined groups of spectra separate from each other (Table 2). After each model was generated, a 20% leave-out cross-validation process was performed with the software. We had also classified the obtained spectra from early-stage PD (ePD) and early-stage MSA (eMSA) by SVM, which resulted in cross-validation accuracy of about 90% (Table 2). Thus, patients with ePD or eMSA were well separated by SVM with better cross-validation accuracy than the patients with PD or MSA in early and more advanced stages combined. It was also unexpected that when the first and second cohorts were combined, the cross-validation score was extremely high between PD and MSA (Table 2). For SVM training, the ClinProtools software had selected several features to enable an efficient model generation by a designated algorithm. The features selected automatically by this software differed from 12 to 24 peaks in each analysis.

Detecting Useful Peaks for Differential Diagnosis between PD and MSA

When spectra were compared between subject groups, the discriminatory peaks were ranked according to the *P* value of a Wilcoxon rank sum test by

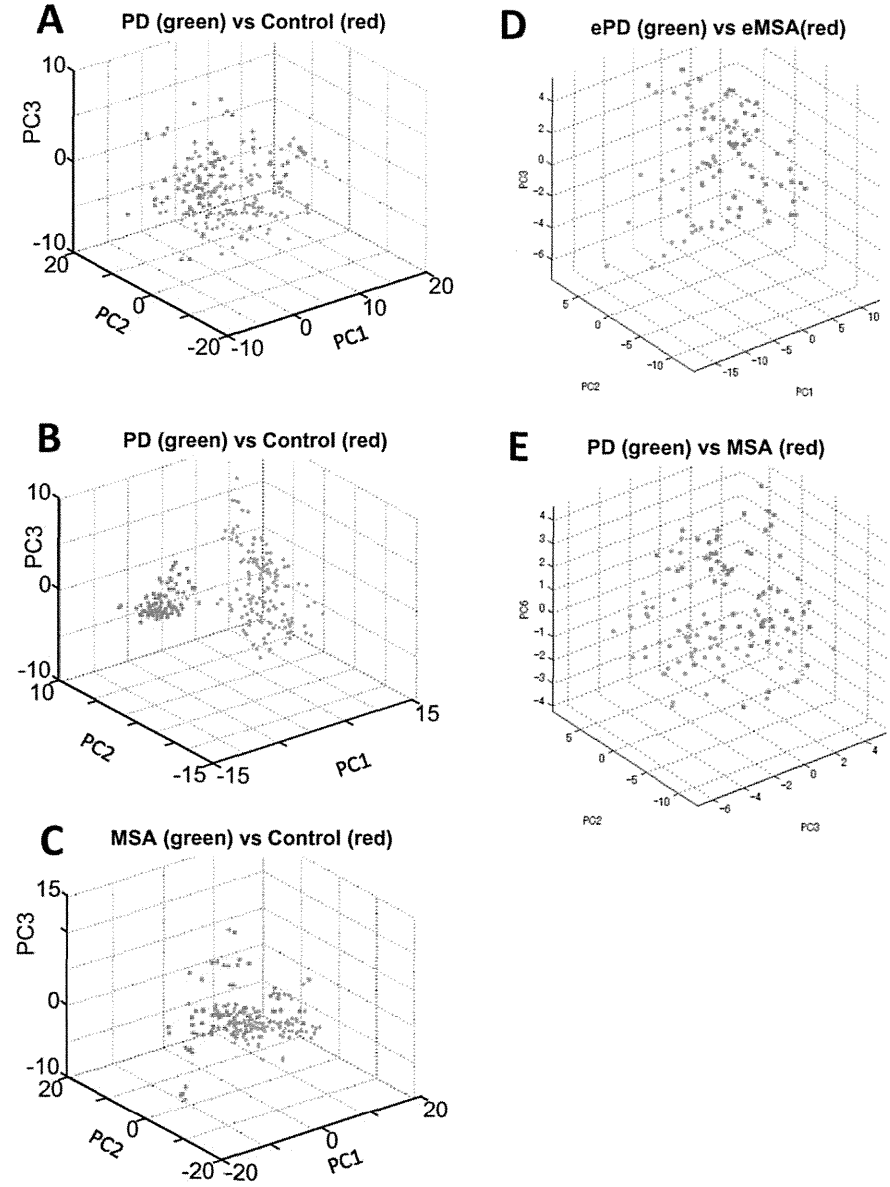

FIG. 1. PCA analyses of CSF proteomic profiles for the discrimination of the 2 indicated groups **(A–E)** displayed as scores on plots (PC, principal component). **A:** PD (green) versus control (red) from the first cohort. **B:** PD (green) versus control (red) from the first and second combined data sets. **C:** MSA (green) versus control (red) from the first cohort. **D:** PD of early-stage samples (ePD) from the first cohort (green) vesus MSA of early-stage samples (eMSA) from the first cohort (red). **E:** PD (green) versus MSA (red) from the second cohort.

ClinProTools. Among the 3 top-ranked peaks in the discrimination of each of the 3 pairs of comparisons, only the peak at *m/z* 6250 was commonly selected in all 3 pairs. The peak at *m/z* 6250 was highly expressed in control patients, but less expressed in PD patients and expressed the least in MSA patients (Fig. 2). In addition, the same respective order of the intensities of that peak was also observed for control, and early-stage patients with PD or MSA (control > ePD > eMSA). ROC curve analysis also proved the diagnostic capability of the peak at *m/z* 6250. The values of the AUC were 0.669 in PD versus control, 0.826 in MSA versus control, and 0.763 in PD versus MSA (Fig. 2B–D, respectively). In the ROC analyses of ePD or eMSA, the AUC values were 0.658 in ePD versus control, 0.886 in eMSA versus control, and 0.956 in ePD versus eMSA (Fig. 2F–H, respectively), suggesting that patients with ePD or eMSA were well discriminated by the peak at *m/z* 6250.

TABLE 2. Cross-validation (%) calculated by the SVM

Differential diagnosis	1st–1	1st–2	1st–3	1st + 2nd (2nd)
PD versus control	85.1	90.3	83.5	98.2 (ND)
MSA versus control	91.9	93.3	90.9	96.7 (ND)
PD versus MSA	85.7	83.8	86.2	90.2 (96.9)
Early PD versus early MSA	89.3	91.5	90.5	ND (ND)

1st–1, 1st–2, and 1st–3, results of 3 independent data analyses for the first cohort samples, taken on 3 different experimental days; early PD, early MSA, patients with disease duration less than 3 years after onset (only nominated in the first cohort); 1st, first cohort; 2nd, second cohort; 1^{st} + 2^{nd}, combining the data sets from the first and second cohorts; ND, not detected (because of a lack of data set information).

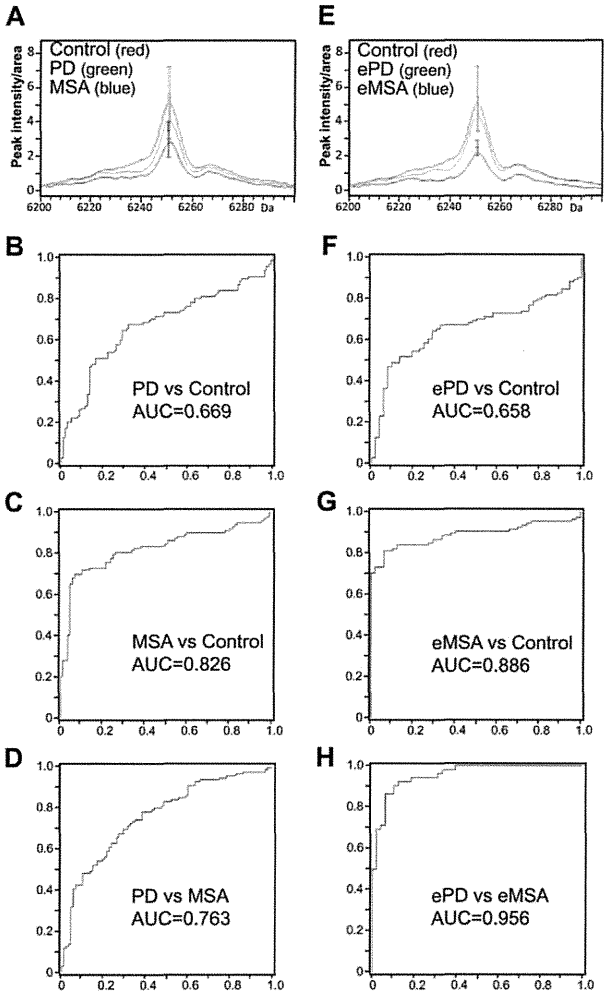

FIG. 2. Mean spectral features at *m/z* 6250 derived from CSF peptide profiling (**A, E**). Bars indicate average values with standard deviation. **B–D, F–H:** ROC curves with an AUC value of peak *m/z* 6250 in the discrimination of the indicated 2 groups (ePD/eMSA, early-stage patients with PD/MSA).

Classification Accuracy by SVM Was Tested for the First and Second Cohorts

The PCA analysis showed that patients with PD or MSA in the first cohort could be efficiently differentiated by their proteomic profiles and also by the peak intensities of the most discriminative peak, at *m/z* 6250. The differentiation ability of proteomic profiling by ClinProTools was put to practical use for the differential diagnosis of PD and MSA. We constructed the classification model to discriminate the groups of PD and MSA patients by using SVM in the training set (Table 3). In this analysis, ClinProTools selected several features identified as useful to classify PD or MSA automatically. Table 3 shows the results of the positive predictive values for MSA and PD (80.0% and 90.0%, respectively), sensitivities (88.9% and 81.8%, respectively), and specificities (81.8% and 88.9%, respectively), when we used the first cohort to build a SVM classifier and test on the second cohort. This process was further validated vice versa, namely, the classification model was generated by the second cohort and was validated on the first cohort. The result was well replicated, but a little lessened for the positive predictive value for MSA, partly because the first cohort contained larger numbers of samples with a variety of clinical situations. However, in both cases, the positive predictive value for PD was more than 80%, indicating that this classification model can efficiently discriminate patients with PD from those with MSA for the other data set.

Discussion

In this study, we have clarified that CSF proteomic profiles could differentiate patients with MSA or PD from each other, even if those with either disease were in the early stage of the illness. ClinProt is a well-established proteomics method that enables proteomic profiling by using the bioinformatics software ClinProTools, which provides algorithms of multivariate statistical analyses.[12,13,14] First by using PCA, we succeeded in differentiating PD, MSA, and the control by the dimension reduction approach. In the next step, we tried to make a classification based on a supervised machine-learning method, SVM. From the first cohort, we have shown that we can classify PD versus MSA with several features selected by SVM. The accuracy was validated by the second cohort, and this step was replicated vice versa. Furthermore, the classification efficiency of SVM and the discrimination power of a data set were proven by ROC analysis. When the number of features is large and the number

TABLE 3. Results of SVM model accuracy tested for the first and second cohorts

Model data set	Validation data set	Clinical diagnosis	Correct rate	Predictive value (%)	Sensitivity (%)	Specificity (%)
1st[a]	2nd	MSA	8/9	80.0	88.9	81.8
		PD	9/11	90.0	81.8	88.9
2nd[b]	1st	MSA	18/22	72.0	81.8	73.1
		PD	19/26	82.6	73.1	81.8

[a]Feature selected for first cohort, 24 peaks, automatically selected by the SVM of the ClinProTools software;
[b]feature selected for second cohort, 12 peaks, automatically selected by the SVM of the ClinProTools software; correct rate, number of truly classified cases for each data set. Sensitivity was calculated as the ratio of true positives against the total number of true-positive and false-negative cases. Specificity was calculated as the ratio of true negatives against the total numbers of true negatives and false positives. Predictive value means the proportion of patients with a positive test who have a disease and was calculated as the ratio of true positives against the total number of true positives and false positives.

of training patterns is comparably small, classification accuracy and the risk of a data-overfitting issue are potential drawbacks. However, this is the first report that has demonstrated the feasibility of the multivariate proteome profiling of CSF obtained from patients with parkinsonian disorders.

Accurate clinical diagnosis of PD and other parkinsonian disorders during life, especially in the early stages of the illness, is surprisingly difficult.[1–4] This unfortunate situation indicates that the development of reliable peptide/protein biomarkers in living subjects would represent a major advance. For example, CSFα-synuclein is so far considered the leading candidate as a single biomarker and has been tested the most extensively. However, published data on the CSF concentration of α-synuclein in patients with PD and controls have been contradictory.[5,6] A recent study clearly showed that CSF α-synuclein decreases in both PD and MSA patients and therefore cannot be used to differentiate these 2 diseases.[17] Similarly, the potential of other CSF proteins previously reported as differentiating biomarkers for parkinsonian disorders has not yet been validated.[5,6,8] A single biomarker may not be sufficient to differentiate PD and MSA by the targeted approach, possibly because of heterogeneity in each disease pathology and pathological overlaps between these 2 disorders.[18] Meanwhile, the combined assessment of multiple biomarkers has been shown to enhance the diagnostic power in neurodegenerative disorders.[19,20] Moreover, a diagnostic panel of multiple CSF proteins, including DJ-1, α-synuclein, Aβ peptides, and tau proteins was demonstrated to aid in Parkinson's disease diagnosis.[21] With these emerging multiple biomarker studies for parkinsonian disorders, we adopted an unbiased approach provided by full MALDI mass spectral profiles based on nontryptic CSF peptides/proteins.

Our results demonstrated a clear separation of PD, MSA, and controls from each other, with good values for cross-validation. In our results, PCA, an unsupervised leaning method to reduce data dimension, demonstrated that PD, MSA, and the control were clearly discriminated from each other by their proteomic profile distributions, and this discrimination was achieved not by a single or a few peaks, but by a combined set of many peaks, namely, the pattern unique to each disease condition. There was no significant association between the clinical variables such as age and sex. In our case, the 3 groups—PD, MSA, and the control—were age-matched as shown in Table 1. The PD group had a larger standard deviation of the ages than those for the MSA group, and we evaluated the PD group for age greater than 65 and age younger than 65 and then compared those 2 groups. However, age had no association with proteomic data, with a cross-validation rate of less than 50%. Sex had no association with proteomic data in each pair of these 3 groups, with a cross-validation rate of less than 50%. For the differential diagnosis of patients with PD and those with MSA, we made an SVM classification model based on a supervised machine-learning method with several features selected by using multiple peaks in the spectra obtained from the blinded test set. When we tested the second cohort of samples on this diagnostic panel, the discriminability of the differential diagnosis groups was clear, with reasonably high sensitivity and specificity, both of which were more than 80% with several features selected. Feature selection can be modulated, and for the current analysis, we adopted about 10–20 peaks for each model generation.

ClinProTools identified the peak at *m/z* 6250 that provided a satisfactory AUC value in the ROC analysis (0.956) only in discrimination of the early-stage patients with PD or MSA, but there were not enough values of this type in the discrimination of other pairs among PD, MSA, and control. From the results of this study, we emphasize that the proteomic pattern, not a single peak, could be a useful diagnostic panel for the differentiation of PD and MSA, even in the early stages. We do not know from which protein the peak at *m/z* 6250 was derived. Previously, Constantinescu et al reported a study of proteomic profiling of CSF in parkinsonian disorders by using SELDI-TOF MS and identified a fragment of chromogranin B, detected as the peak at *m/z* 6250 as a peptide to help differentiate patients with PD and MSA.[11] The peak intensity of the chromogranin B–derived fragment decreased in MSA patients compared with PD patients in their study. The chromogranins are widely distributed in neuroendocrine and nervous system tissues.[22] They suggested that the decrease in chromogranin B–derived fragments in MSA could be related to more aggressive synaptic or neuronal loss in patients with MSA than what is observed in PD.[11] For the moment, we will not explore this possibility any further because single-peak identification was not a top priority compared with testing reproducibility with a larger patient population and fine-tuning the comprehensive diagnostic panel based on these data.

In conclusion, although our results were derived from limited sample numbers, our study is the first to identify a promising application of proteomic pattern analysis to the clinical diagnosis of PD and MSA by profiling their respective CSF proteomes. Further studies are needed to confirm our current findings in larger cohorts of parkinsonian patients, especially to help diagnose disease progression and improve therapeutic efficacy. ■

Acknowledgments: We thank Drs. Yuichi Tokuda and Kengo Yoshii for useful discussion in the statistical analysis.

References

1. Hughes AJ, Daniel SE, Kilford L, Lees AJ. Accuracy of clinical diagnosis of idiopathic Parkinson's disease: a clinico-pathological study of 100 cases. J Neurol Neurosurg Psychiatry 1992;55: 181–184.

2. Stefanova N, Bucke P, Duerr S, Wenning GK. Multiple system atrophy: an update. Lancet Neurol 2009;8:1172–1178.
3. Gilman S, Wenning GK, Low PA, et al. Second consensus statement on the diagnosis of multiple system atrophy. Neurology 2008;71:670–676.
4. Brooks DJ, Seppi K. Proposed neuroimaging criteria for the diagnosis of multiple system atrophy. Mov Disord 2009;24:949–964.
5. Tokuda T, Salem SA, Allsop D, et al. Decreased alpha-synuclein in cerebrospinal fluid of aged individuals and subjects with Parkinson's disease. Biochem Biophys Res Commun 2006;349:162–166.
6. Hong Z, Shi M, Chung KA, et al. DJ-1 and alpha-synuclein in human cerebrospinal fluid as biomarkers of Parkinson's disease. Brain 2010;133:713–726.
7. Abdo WF, De Jong D, Hendriks JC, et al. Cerebrospinal fluid analysis differentiates multiple system atrophy from Parkinson's disease. Mov Disord 2004;19:571–579.
8. Brettschneider J, Petzold A, Sussmuth SD, et al. Neurofilament heavy-chain NfH (SMI35) in cerebrospinal fluid supports the differential diagnosis of Parkinsonian syndromes. Mov Disord 2006; 21:2224–2227.
9. Abdi F, Quinn JF, Jankovic J, et al. Detection of biomarkers with a multiplex quantitative proteomic platform in cerebrospinal fluid of patients with neurodegenerative disorders,. J Alzheimers Dis 2006;9:293–348.
10. Zhang J, Sokal I, Peskind ER, et al. CSF multianalyte profile distinguishes Alzheimer and Parkinson diseases. Am J Clin Pathol 2008; 129:526–529.
11. Constantinescu R, Andreasson U, Li S, et al. Proteomic profiling of cerebrospinal fluid in parkinsonian disorders. Parkinsonism Relat Disord 2010;16:545–549.
12. Ketterlinus R, Hsieh SY, Teng SH, Lee H, Pusch W. Fishing for biomarkers: analyzing mass spectrometry data with the new ClinProTools software. Biotechniques 2005;Suppl:37–40.
13. Bosso N, Chinello C, Picozzi SC, et al. Human urine biomarkers of renal cell carcinoma evaluated by ClinProt. Proteomics Clin Appl 2008;2:1036–1046.
14. Komori M, Matsuyama Y, Nirasawa T, et al. Proteomic pattern analysis discriminates among multiple sclerosis-related disorders. Ann Neurol 2011;doi:10.1002/ana.22633.
15. Ivosev G, Burton L, Bonner R. Dimensionality reduction and visualization in principal component analysis. Anal Chem 2008;80: 4933–4944.
16. Sekiyama E, Matsuyama Y, Higo D, et al. Applying magnetic bead separation/MALDI-TOF mass spectrometry to human tear fluid proteome analysis. J Proteomics Bioinformatics 2008;1: 368–373.
17. Mollenhauer B, Locascio JJ, Schulz-Schaeffer W, Sixel-Doring F, Trenkwalder C, Schiossmacher MG. α-Synuclein and tau concentrations in cerebrospinal fluid of patients presenting with parkinsonism: a cohort study. Lancet Neurol 2011;10:230–240.
18. van Dijk KD, Teunissen CE, Drukarch B, et al. Diagnostic cerebrospinal fluid biomarkers for Parkinson's disease: a pathogenetically based approach. Neurobiol Dis 2010;39:229–241.
19. Fagan AM, Roe CM, Xiong C, Mintun MA, Morris JC, Holyzman DM. Cerebrospinal fluid tau/beta-amyloid(42) ratio as a prediction of cognitive decline in nondemented older adults. Arch Neurol 2007;64:343–349.
20. Shaw LM, Vanderstichele H, Knapik-Czajka M, et al. Alzheimer's Disease Neuroimaging Initiative. Cerebrospinal fluid biomarker signature in Alzheimer's disease neuroimaging initiative subjects. Ann Neurol 2009;65:403–413.
21. Shi M, Bradner J, Hancock AM, et al. Cerebrospinal fluid biomarkers for Parkinson disease diagnosis and progression. Ann Neurol 2011;69:570–580.
22. Helle KB. The granin family of uniquely acidic proteins of the diffuse neuroendocrine system: comparative and functional aspects. Biol Rev Camb Philos Soc 2004;79:769–794.